

Heterogeneous Crystal Nucleation: The Effect of Lattice Mismatch

Gyula I. Tóth,¹ György Tegze,¹ Tamás Pusztai,¹ and László Gránásy^{1,2}

¹Research Institute for Solid State Physics and Optics, P.O. Box 49, H-1525 Budapest, Hungary

²BCAST, Brunel University, Uxbridge, Middlesex, UB8 3PH, United Kingdom

(Received 28 October 2011; published 11 January 2012)

A simple dynamical density functional theory is used to investigate freezing of an undercooled liquid in the presence of a crystalline substrate. We find that the adsorption of the crystalline phase on the substrate, the contact angle, and the height of the nucleation barrier are nonmonotonic functions of the lattice constant of the substrate. We show that the free-growth-limited model of particle-induced freezing by Greer *et al.* [*Acta Mater.* **48**, 2823 (2000)] is valid for larger nanoparticles and a small anisotropy of the interface free energy. Faceting due to the small size of the foreign particle or a high anisotropy decouples free growth from the critical size of homogeneous nuclei.

DOI: 10.1103/PhysRevLett.108.025502

PACS numbers: 81.10.Aj, 64.60.Q-, 64.70.dg, 68.35.Rh

Nucleation is the early stage of first-order phase transitions, in which fluctuations drive the system towards the new phase. The height of the nucleation barrier is usually reduced by heterogeneities (walls, floating particles, templates, etc.), a phenomenon termed *heterogeneous* nucleation [1]. The efficiency of the heterogeneities in instigating freezing is influenced by a range of microscopic properties, such as crystal structure, lattice mismatch, surface roughness, adsorption, etc., which are often condensed into the contact angle used in the classical theory [1] and coarse-grained continuum models [2]. Studies relating such microscopic and macroscopic properties are rare. Recent experiments on colloids explored the effect of configurable seed structures realized by optical tweezers on nucleation, and indicate that the defect structure generated by the seed governs the morphology of the growing crystals [3]. The simulation methods used in addressing the interaction of heterogeneities with the crystallizing liquid include *ab initio* molecular dynamics (AIMD), molecular dynamics (MD), Monte Carlo (MC), and dynamical density functional techniques (DDFT). A DDFT study mapped out the effect of seed structures on crystallization in 2D [4]. MD and MC simulations explored the interaction between a foreign wall and a crystallizing fluid [5–10]. The unstructured wall is nearly wet by the (111) face of the hard-sphere crystal, and the results can only be interpreted if line tension is also taken into account [5], a result recovered within the lattice gas model [7]. Freezing on walls patterned on the atomic scale has been investigated for triangular and square lattices, zigzag stripe, and rhombic surface patterns [6]. The presence of a wall is shown to lead to ordering in the adjacent liquid layers [8] that influences the adsorption of crystalline molecule layers at the surface of the substrate. Owing to reduced stress, nanoscale pits in an amorphous wall proved to be a more efficient nucleation site than pits in a crystalline wall [9]. Recent MD and AIMD work for the AlTiB system indicates the formation of crystalline layers on appropriate surfaces of the Al₃Ti and TiB₂ substrates

[10,11]. These phenomena, especially the effect of lattice mismatch, are crucial from the viewpoint of the highly successful free-growth-limited model of particle-induced freezing by Greer and co-workers [1,12], a model in which cylindrical particles, whose circular faces (of radius R) are ideally wet by the crystal, remain dormant during cooling until the radius of the homogeneous nuclei becomes smaller than R , and free growth sets in. The microscopic studies are limited in time and space. Part of these limitations can be overcome by a simple DDFT, termed the phase-field crystal (PFC) model [13], which works on the diffusive time scale and can handle systems containing as many as 2.4×10^7 atoms [14]. The model has been supplemented with suitable potential energy terms [14,15] or boundary conditions [16] to represent foreign walls.

Herein, we present a systematic atomic scale study relying on the PFC model, which explores the role lattice mismatch plays in heterogeneity-induced freezing of undercooled liquids.

The free energy of the heterogeneous system reads as

$$F = \int dV \left\{ \frac{\psi}{2} [-\epsilon + (1 + \nabla^2)^2] \psi + \frac{\psi^4}{4} + \psi V(\mathbf{r}) \right\}, \quad (1)$$

where $\psi \propto (\rho - \rho_L^{\text{ref}})/\rho_L^{\text{ref}}$ is the scaled density difference relative to the reference liquid of particle density ρ_L^{ref} , and the parameter $\epsilon > 0$ is the reduced temperature related to the bulk moduli of the liquid and the crystalline phases. Here $V(\mathbf{r}) = [V_{s,0} - V_{s,1}S(a_s, \mathbf{r})]f(\mathbf{r})$, where $V_{s,0}$ tunes adsorption of crystal layers, $V_{s,1}$ is the amplitude of the periodic part of the potential, the single-mode function $S(a_s, \mathbf{r})$ [14] sets the structure, and a_s is the lattice constant of the substrate. The size and shape of the substrate are defined by the envelope function $f(\mathbf{r}) \in [0, 1]$.

In the PFC model, heterogeneous nucleation (much like homogeneous nucleation [17]) can be addressed following two routes: (i) via simulations based on the equation of motion (EOM) or (ii) by finding the relevant equilibria via solving the Euler-Lagrange equation (ELE). Here we use

both routes. The dimensionless ELE and EOM of the PFC model read as $\frac{\delta \mathcal{F}}{\delta \psi} = (\frac{\delta \mathcal{F}}{\delta \psi})_{\psi_0}$ and $\frac{\partial \psi}{\partial \tau} = \nabla^2 \frac{\delta \mathcal{F}}{\delta \psi} + \zeta$, respectively, where $\frac{\delta \mathcal{F}}{\delta \psi}$ denotes the functional derivative of \mathcal{F} with respect to ψ , and τ is the dimensionless time. The right-hand side of the ELE is taken at the far-field value ψ_0 (homogeneous liquid). In the EOM, the fluctuations are represented by a colored Gaussian noise ζ of correlator $\langle \zeta(\mathbf{r}, \tau) \zeta(\mathbf{r}', \tau') \rangle = -\alpha \nabla^2 g(|\mathbf{r} - \mathbf{r}'|, \sigma) \delta(\tau - \tau')$, where α is the noise strength and $g(|\mathbf{r} - \mathbf{r}'|, \sigma)$ a high frequency cutoff function [18] for wavelengths shorter than the interatomic spacing ($\sigma = \pi\sqrt{6}$). Because of the overdamped conservative dynamics the EOM realizes, the PFC model so defined is suitable for describing crystalline colloidal aggregation [19,20]. These equations have been solved numerically [21] on rectangular grids in 2D and 3D, assuming periodic boundary condition.

The PFC model has stability domains for the homogeneous liquid and triangular crystal in 2D [13], and for the liquid and bcc, hcp, and fcc phases in 3D [14,22]. We work in the liquid-triangular and liquid-bcc coexistence regimes; i.e., the fcc and hcp phases are metastable (MS). The anisotropy of the solid-liquid interface free energy increases with ϵ [15,20]: at $\epsilon = 0.25$ γ has a small anisotropy as for metals, while for $\epsilon = 0.5$ faceted crystal-liquid interfaces form, as in some 2D colloids [23].

First, we study heterogeneous nuclei forming in 2D on a flat square-lattice wall of varied lattice constant using the ELE method described in Ref. [14] (the free-energy surface has many local minima allowing the ELE to map out the nucleation barrier). The two dominant relative orientations observed in dynamic (EOM) simulations are considered [15]: $(01\bar{1})$ or $(11\bar{2})$ parallel with the wall. In the case of weak anisotropy ($\epsilon = 0.25$), the contact angle is defined as the angle between the linear and circular parts of the closed contour line corresponding to $(\psi_L + \psi_S)/2$ in the coarse-grained (finite impulse response filtered [24]) particle density [see Figs. 1(a) and 1(b)]. (Subscripts S and L stand for solid and liquid.) We observe a nonmonotonic relationship between the contact angle and a_s [Fig. 1(c)]. In the case of faceted interfaces ($\epsilon = 0.5$), the contact angle is 60° for the orientation $(01\bar{1})$ parallel to the wall [Fig. 1(d)], whereas it is 90° for $(11\bar{2})$ parallel to the wall [Fig. 1(e)], independently of the monolayer sometimes forming on the wall. As in Ref. [14], the work of formation fits well to the classical $W(l) = Al^2 + Bl$ relationship, where l is the linear size of the nucleus. Accordingly, the barrier height (W^*) has been defined as the maximum of the fitted formula. W^* data obtained so for the two orientations are shown for $1/2 < a_s/\sigma \leq 2$ in Fig. 1(f). The W^* vs a_s/σ relationships are nonmonotonic and have deep minima for the matching lattice constants ($a_s/\sigma = 1$ and $\sqrt{3}$). Except for $\sim 1.7 < a_s/\sigma \leq 2$, nuclei of orientation of $(01\bar{1})$ parallel with the wall dominate.

Next, we investigate the free-growth-limited mechanism in 2D on square-shaped particles at reduced temperatures

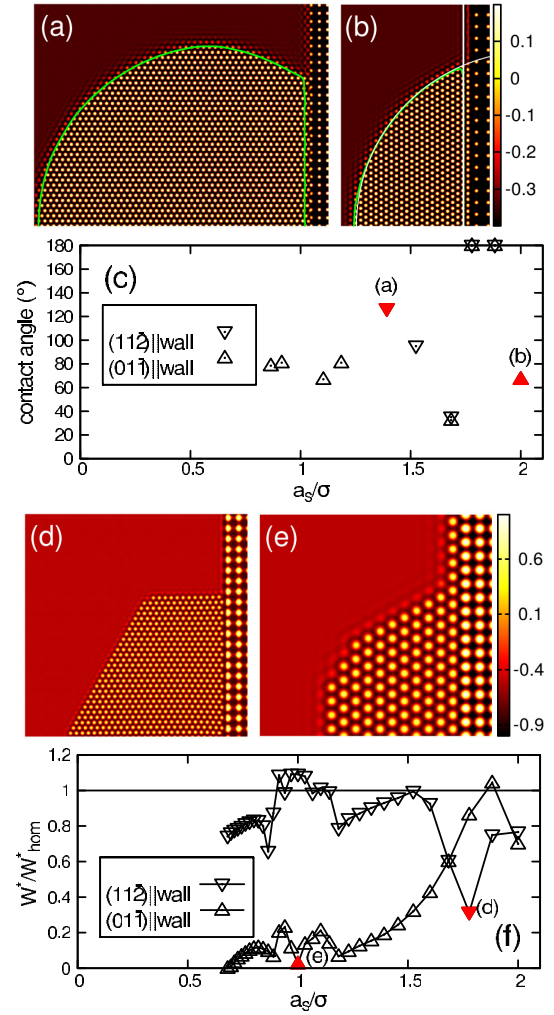


FIG. 1 (color online). Heterogeneous crystal nucleation on a flat wall in 2D from solving ELE. (a),(b) Typical (nonfaceted) nuclei obtained for $\epsilon = 0.25$, $\psi_0 = -0.341$, $V_{s,0} = 0.5$, and $V_{s,1} = 0.5$. Here $a_s/\sigma = 1.49$ and 2.0 , respectively, while the orientations are $(11\bar{2})$ and $(01\bar{1})$ parallel with the wall. The intersection of the circular and linear fits (white lines) to the contour line [gray (green) line] defines the contact angle. (c) Contact angle versus a_s/σ for $\epsilon = 0.25$, $\psi_0 = -0.341$. (d),(e) Typical (faceted) nuclei obtained for $\epsilon = 0.5$, $\psi_0 = -0.51415$, $V_{s,0} = 0$, $V_{s,1} = 0.65$, and $a_s/\sigma = \sqrt{3}$ and 1.0 . Respective orientations: $(11\bar{2})$ and $(01\bar{1})$ parallel with the wall. (f) Work of formation of faceted nuclei normalized by the value for homogeneous nucleation (W^*/W_{hom}^*) vs a_s/σ for $\epsilon = 0.5$ and $\psi_0 = -0.51415$.

$\epsilon = 0.25$ and 0.5 . To ensure nearly perfect wetting, a precondition of the free-growth-limited model [12], we set $a_s = \sigma$. Two linear sizes have been used: $L_s = 4\sigma$ and $L_s = 32\sigma$. The results for $L_s = 32\sigma$ and $\epsilon = 0.25$ indicate that even outside of the coexistence region adsorbed crystal layers form on the substrate [Fig. 2(a)], which evolve to circular caps inside the coexistence region [Fig. 2(b)]. When the diameter of the homogeneous nucleus becomes smaller than L_s , free growth commences

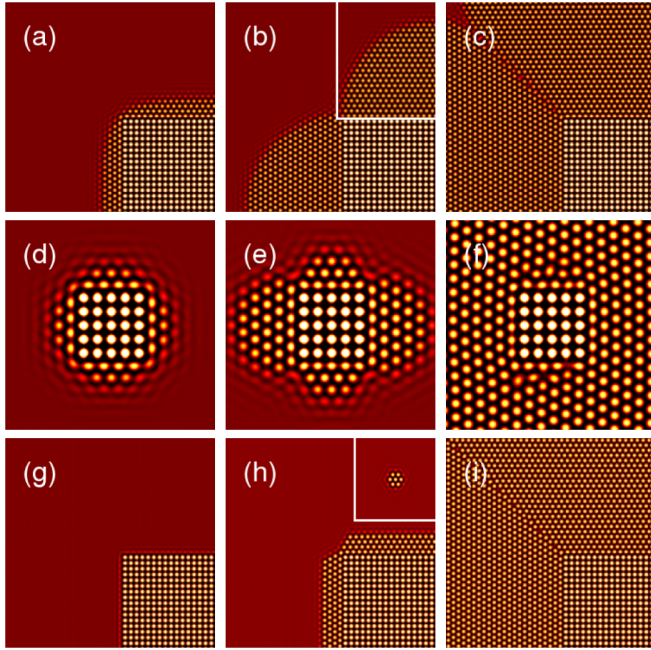


FIG. 2 (color online). Free-growth-limited crystallization in 2D. Adsorption of the crystalline phase on square-shaped foreign particles as predicted by ELE as a function of liquid density, reduced temperature, and size. (a)–(c) $\epsilon = 0.25$ and $L_s = 32\sigma$; $\psi_0 = -0.3418$, -0.3405 , and -0.3404 , respectively. (d)–(f) $\epsilon = 0.25$ and $L_s = 4\sigma$; $\psi_0 = -0.3426$, -0.3363 , and -0.3359 , respectively. (g)–(i) $\epsilon = 0.5$ and $L_s = 32\sigma$; $\psi_0 = -0.5190$, -0.4939 , and -0.4929 , respectively. In all cases $a_s/\sigma = 1$, $V_{s,0} = 0$, and $V_{s,1} = 0.65$. The insets show the respective homogeneous nuclei.

[Fig. 2(c)]. This observation is in excellent agreement with the free-growth-limited model [12]. For the smaller L_s , however, a faceted crystal shape is observed, and the free-growth limit is reached at a monatomic critical size that is much smaller than L_s [Figs. 2(d)–2(f)]. At $\epsilon = 0.5$, faceted crystals form [Figs. 2(g)–2(i)]. Here, free growth takes place when the critical size is much smaller than $L_s = 32\sigma$. These findings indicate that the free-growth-limited mechanism is valid as long as the foreign particles are sufficiently large, and the free energy of the solid-liquid interface has only a weak anisotropy.

We study the effect of lattice mismatch on crystal adsorption in 2D at $\epsilon = 0.25$ and $\psi_0 = -0.34045$. The lattice constant of the substrate is varied between $\sigma/2$ and 2σ , so that it stays commensurable with $L_s = 32\sigma$. The results are summarized in Fig. 3. As for the flat wall, the amount of crystal adsorbed on the particle is a non-monotonic function of a_s . At $a_s = \sigma$ nearly semicircular adsorbates appear on the faces of the particle [Fig. 3(c)], while for slightly different a_s values much thinner crystal layers are observed on both sides [Fig. 3(g)]. Further away from $a_s = \sigma$, the adsorbed layer thickens; yet for $a_s \approx 2\sigma$ crystal adsorption is forbidden.

We extend the study of the free-growth-limited model to 3D, using a cube shaped foreign particle of simple cubic

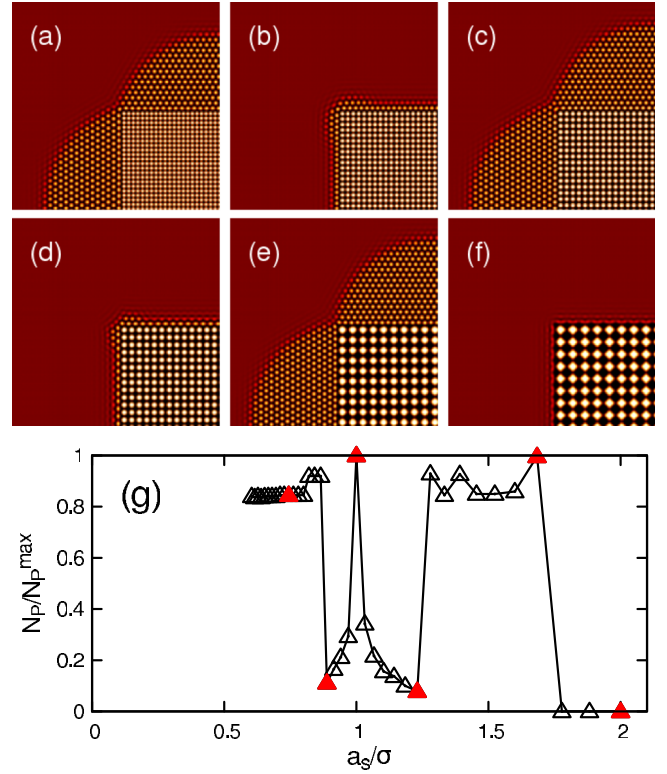


FIG. 3 (color online). Adsorption of the crystalline phase in 2D on square-shaped particles versus mismatch at $\epsilon = 0.25$, $\psi_0 = -0.34045$, $V_{s,0} = 0$, and $V_{s,1} = 0.65$. (a)–(f) Equilibrium states from solving ELE on 1024×1024 grid; $a_s/\sigma = 0.74$, 0.89 , 1.00 , 1.23 , 1.68 , and 2.00 , respectively. (g) Number of adsorbed crystalline particles normalized by their maximum versus lattice constant. Full symbols denote results corresponding to (a)–(f).

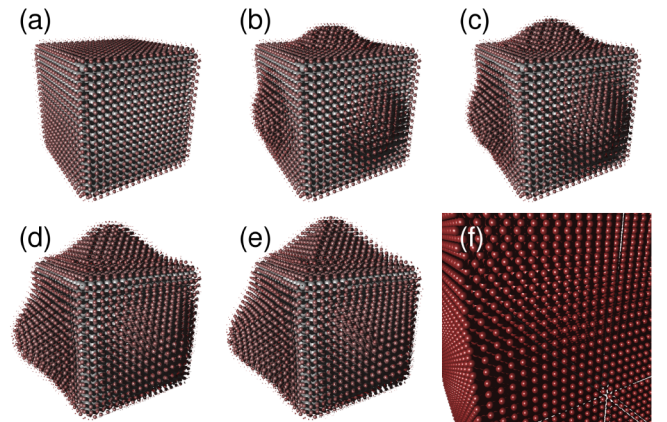


FIG. 4 (color online). Free-growth-limited crystallization in 3D on a cube of sc structure. $\epsilon = 0.25$ and $\psi_0 = -0.3538$, -0.3516 , -0.3504 , -0.3489 , -0.3482 , and -0.3480 , respectively, whereas $L_s = 16a_{\text{bcc}}$, and a_{bcc} is the lattice constant of the stable bcc structure. $V_{s,0} = 0$ and $V_{s,1} = 0.65$. (ELE has been solved on a $256 \times 256 \times 256$ grid.) Spheres centered on density peaks are shown, whose size increases with the height of the peak. Color varies with peak height, interpolating between red (minimum height) and white (maximum height).

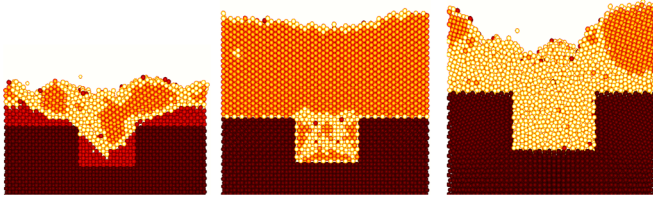


FIG. 5 (color online). Freezing on fcc substrate with a rectangular nanoscale pit (EOM in 3D). Spheres drawn around density peaks larger than $\psi = 0.05$ are shown. Order parameters q_4 and q_6 are used for structural analysis (see Ref. [17]). Hues from dark to light stand for the substrate and the (MS) fcc, bcc, and (MS) amorphous structures, respectively. ($\epsilon = 0.16$, $\psi_0 = -0.25$, $\alpha = 0.42$; grid size: $512 \times 256 \times 256$; $\Delta x = 2\pi/8$, and $\Delta\tau = 0.5774$, $V_{s,0} = 0$, and $V_{s,1} = 0.25$.) From left to right $a_s/a_{fcc} = 1.0$, 1.098, and 1.42. Cross-sectional views are displayed.

(sc) structure and a_s coinciding with the lattice constant of the bcc structure, known to yield bcc freezing [25]. The results are in a qualitative agreement with the free-growth-limited model [1] (Fig. 4).

Behavior consistent with previous EOM work [17,25] is observed on a fcc substrate with a rectangular pit (Fig. 5): For matching a_s , one finds fcc and bcc epitaxy interfered by edge-induced frustration. At high mismatch, amorphous-phase-mediated bcc freezing occurs, adding to the complexity observed in MD studies [9].

In summary, we used the phase-field crystal model to study heterogeneity-induced crystalline freezing in 2D and 3D. Our results extend previous knowledge in the following directions: (i) The mismatch between the substrate and the crystal influences nonmonotonically the contact angle, the adsorption of the crystalline phase, and heterogeneous nucleation; (ii) within atomistic theory, we have confirmed the validity of the free-growth-limited model of particle-induced freezing by Greer *et al.* [12] for larger nanoparticles ($L_s \geq 32\sigma$) and small anisotropy of the solid-liquid interface free energy. However, for small nanoparticles ($L_s \sim 4\sigma$) or high anisotropies, the critical supersaturation substantially deviates from the one expected from analytic theory [12]. Note that these results are independent of the dynamics assumed.

This work is expected to instigate further experiments on colloid systems and demonstrates the flexibility of the PFC approach in modeling nanoscale self-assembly.

This work has been supported by the EU FP7 Projects “ENSEMBLE” (NMP4-SL-2008-213669) and “EXOMET,” the latter co-funded by ESA, and by the ESA MAP/PECS project “MAGNEPHAS III.”

[1] K.F. Kelton and A.L. Greer, *Nucleation in Condensed Matter* (Elsevier, Amsterdam, 2010).

- [2] L. Gránásy, T. Pusztai, D. Saylor, and J. A. Warren, *Phys. Rev. Lett.* **98**, 035703 (2007); H. Ding and P. D. M. Spelt, *Phys. Rev. E* **75**, 046708 (2007); J. A. Warren, T. Pusztai, L. Körmeyi, and L. Gránásy, *Phys. Rev. B* **79**, 014204 (2009).
- [3] M. Hermes, E. C. M. Vermolen, M. E. Leunissen, D. L. J. Vossen, P. D. J. van Oostrum, M. Dijkstra, and A. van Blaaderen, *Soft Matter* **7**, 4623 (2011).
- [4] S. van Teeffelen, C. N. Likos, and H. Löwen, *Phys. Rev. Lett.* **100**, 108302 (2008).
- [5] S. Auer and D. Frenkel, *Phys. Rev. Lett.* **91**, 015703 (2003).
- [6] A. Esztermann and H. Löwen, *J. Phys. Condens. Matter* **17**, S429 (2005).
- [7] D. Winter, P. Virnau, and K. Binder, *Phys. Rev. Lett.* **103**, 225703 (2009).
- [8] E. B. Webb III, G. S. Grest, and D. R. Heine, *Phys. Rev. Lett.* **91**, 236102 (2003); S. Toxvaerd, *J. Chem. Phys.* **117**, 10 303 (2002).
- [9] J. A. van Meel, R. P. Sear, and D. Frenkel, *Phys. Rev. Lett.* **105**, 205501 (2010).
- [10] J. Wang, A. Horsfield, P. D. Lee, and P. Brommer, *Phys. Rev. B* **82**, 144203 (2010).
- [11] J. Wang, A. Horsfield, U. Schwingenschlögl, and P. D. Lee, *Phys. Rev. B* **82**, 184203 (2010).
- [12] A. L. Greer, A. M. Brunn, A. Tronche, P. V. Evans, and D. J. Bristow, *Acta Mater.* **48**, 2823 (2000); T. E. Quedsted and A. L. Greer, *Acta Mater.* **53**, 2683 (2005).
- [13] K. R. Elder, M. Katakowski, M. Haataja, and M. Grant, *Phys. Rev. Lett.* **88**, 245701 (2002).
- [14] G. I. Tóth, G. Tegze, T. Pusztai, G. Tóth, and L. Gránásy, *J. Phys. Condens. Matter* **22**, 364101 (2010).
- [15] L. Gránásy, G. Tegze, G. I. Tóth, and T. Pusztai, *Philos. Mag.* **91**, 123 (2011).
- [16] R. Prieler, J. Hubert, D. Li, B. Verleye, R. Haberkern, and H. Emmerich, *J. Phys. Condens. Matter* **21**, 464110 (2009).
- [17] G. I. Tóth, T. Pusztai, G. Tegze, G. Tóth, and L. Gránásy, *Phys. Rev. Lett.* **107**, 175702 (2011).
- [18] J. G. Ojalvo and J. M. Sancho, *Noise in Spatially Extended Systems* (Springer, New York, 1999), p. 175.
- [19] S. van Teeffelen, C. N. Likos, and H. Löwen, *Phys. Rev. Lett.* **100**, 108302 (2008).
- [20] G. Tegze, L. Gránásy, G. I. Tóth, J. F. Douglas, and T. Pusztai, *Soft Matter* **7**, 1789 (2011); G. Tegze, G. I. Tóth, and L. Gránásy, *Phys. Rev. Lett.* **106**, 195502 (2011).
- [21] G. Tegze, G. Bansal, G. I. Tóth, T. Pusztai, Z. Fan, and L. Gránásy, *J. Comput. Phys.* **228**, 1612 (2009).
- [22] A. Jaatinen and T. Ala-Nissila, *J. Phys. Condens. Matter* **22**, 205402 (2010).
- [23] G. Y. Onoda, *Phys. Rev. Lett.* **55**, 226 (1985); A. T. Skjeltorp, *Phys. Rev. Lett.* **58**, 1444 (1987).
- [24] See W. H. Press, S. A. Teukolsky, W. T. Vetterling, and B. P. Flannery, *Numerical Recipes in FORTRAN* (Cambridge University Press, Cambridge, England, 1992), 2nd ed..
- [25] G. Tegze, L. Gránásy, G. I. Tóth, F. Podmaniczky, A. Jaatinen, T. Ala-Nissila, and T. Pusztai, *Phys. Rev. Lett.* **103**, 035702 (2009).